Materials Science and Engineering C 31 (2011) 983–991

Gel-derived SiO_2–CaO–Na_2O–P_2O_5 bioactive powders: Synthesis and *in vitro* bioactivity

Renato Luiz Siqueira *, Oscar Peitl, Edgar Dutra Zanotto

Programa de Pós-Graduação em Ciência e Engenharia de Materiais, Laboratório de Materiais Vítreos, Departamento de Engenharia de Materiais, Universidade Federal de São Carlos, Rod. Washington Luis km 235, CP 676, 13565–905 São Carlos, SP, Brazil

ARTICLE INFO

Article history:
Received 18 September 2010
Received in revised form 10 January 2011
Accepted 17 February 2011
Available online 24 February 2011

Keywords:
Sol–gel
Bioactive glass-ceramics
SiO_2–CaO–Na_2O–P_2O_5
In vitro tests

ABSTRACT

In the present work, bioactive powders of the quaternary SiO_2–CaO–Na_2O–P_2O_5 system were synthesized by means of a sol–gel route. In their synthesis, tetraethoxysilane ($Si(OC_2H_5)_4$), calcium nitrate tetrahydrate ($Ca(NO_3)_2{\cdot}4H_2O$) and sodium nitrate ($NaNO_3$) were chosen as precursors of SiO_2, CaO and Na_2O, respectively. For P_2O_5, two different precursors were tested: triethylphosphate ($OP(OC_2H_5)_3$) and phosphoric acid (H_3PO_4). The gels were then converted into ceramic powders by heat treatments in the temperature range 700–1000 °C. The resulting materials were characterized by X-ray diffraction (XRD), Fourier transform infrared spectroscopy (FTIR), scanning electron microscopy coupled with energy dispersive spectroscopy (SEM/EDS) and in vitro bioactivity in acellular simulated body fluid (SBF). During the conversion of the gels into ceramics the mineralization behavior of the two sets of samples was different, but all the resulting materials were bioactive. The samples prepared using phosphoric acid exhibited the best in vitro bioactivity. This result was attributed to the preferential formation of bioactive sodium calcium silicate $Na_2Ca_2Si_3O_9$ crystals, especially in the samples submitted to heat treatments at 700 and 800 °C, which could not be observed in the samples prepared using triethylphosphate.

1. Introduction

Bone and dental tissue repair due to traumatisms, infectious processes, neoplasms and congenital malformations is a current challenge to the medical and dental fields. In the early 1970s, a special type of material emerged from the pioneering work of Hench et al. [1] – Bioglass® 45S5 – a glass of the quaternary SiO_2–CaO–Na_2O–P_2O_5 system which, due to its remarkable features of interaction with living tissues, still guides the R&D tendencies in this exciting research field, and created new opportunities for medical and dental treatments [1–4]. It is important to note that, in addition its high bioactivity – i.e., the ability to form *in-situ* a hydroxyapatite (HA) layer on its surface, which promotes an interface and bonds to some living tissues (cartilage and bones) – it has been demonstrated that Bioglass® 45S5 affects osteoblast activity, which ultimately results in enhanced bone formation. Indeed, at least seven families of genes are upregulated when primary human osteoblasts are exposed to the ionic dissolution products of this material, including genes that encode proteins associated with osteoblast proliferation and differentiation [1,4].

The standard method to produce this bioactive glass is by melting a mixture of oxides, carbonates and phosphates and then quenching the molten liquid to form a glass, which is then crushed into a powder when the objective is to obtain the material in particulate form. However, the melting method often leads to chemically heterogeneous materials, with incipient crystallization plus some minor or significant degree of contamination from the solid chemicals and during the melting/cooling/grinding procedures to make a powder. Hence, it has been a long-standing challenge to develop alternative synthesis of bioactive glasses by chemical methods. For instance, in 1991, Li et al. [5] proposed a synthesis of similar bioactive glasses by the sol–gel method, which, in principle, shows several advantages and only a few disadvantages in comparison to the melting and solidification route so far established [6].

The sol–gel method allowed for the production of bioactive glasses with higher purity and homogeneity, and also significantly expanded the ranges of compositions that exhibit bioactivity as compared to bioactive glasses prepared by the traditional method of melting/cooling [3,5,7]. Moreover, because all steps involved in the sol–gel route are carried out at relatively low temperatures, the addition of some components to lower the melting temperature, such as Na_2O or K_2O, which are used in the conventional route, is no longer required. Thus, the use of the sol–gel method in the synthesis of these materials simplified the composition, leading to the first bioactive glasses of the ternary SiO_2–CaO–P_2O_5 system [5,8]. Another important point about Na_2O or K_2O is that, besides reducing the melting temperature of bioactive glasses by the traditional route, their addition to the system makes the final materials more soluble in aqueous media, a factor which is extremely important for the interaction of the material with

* Corresponding author. Tel.: +55 16 3351 8556; fax: +55 16 3361 5404.
E-mail address: rastosfix@gmail.com (R.L. Siqueira).
URL: http://www.lamav.ufscar.br (R.L. Siqueira).

0928-4931/$ – see front matter © 2011 Elsevier B.V. All rights reserved.
doi:10.1016/j.msec.2011.02.018

living tissues [1–4,7,9]. On the other hand, this point is counterbalanced by the high specific surface area of the sol–gel bioactive glasses (around 200 $m^2 g^{-1}$), an intrinsic characteristic of these materials acquired with this synthesis method [3,5,7,9–11].

Since its initial proposal two decades ago, the sol–gel method has been widely tried for bioactive glass syntheses due to its potential advantages in relation to the traditional method. For instance, the possibility of producing new compositions in milder laboratory conditions, containing in their formulations elements such as Zn, Mg, Ag, Sr and Sm is very exciting because this may allow the use of bioactive glasses in some specific applications [11–19]. However, despite these developments in relation to the synthesis procedures, the study of the original quaternary sol–gel bioactive glasses containing Na has been largely unexplored. In 2000, Łączka et al. [20] synthesized materials of the ternary $CaO–P_2O_5–SiO_2$ system by the sol–gel route adding a number of other elements, including Na. But in this case, the studied composition was quite different from the composition of the "golden standard" Bioglass® 45S5, which is still commercially produced by the fusion and solidification process [1]. In 2005, Carta et al. [21] proposed a synthesis method of a new glass of the $P_2O_5–CaO–Na_2O–SiO_2$ system; a phosphate glass with very low concentration of SiO_2 (0–25% in mol). Consequently, the studied composition was also quite distinct from that of Bioglass® 45S5, a material with numerous successful clinical applications.

Another point that should be highlighted is that, besides reducing the melting temperature for glass preparation by the traditional route, the addition of Na in these materials makes them more soluble in aqueous media, as previously mentioned. These features of glassy systems containing Na associated with the high intrinsic surface area of sol–gel glasses can result in a very interesting property that should be further explored, since the dissolution rate of materials designed for implants is a fundamental factor for their interaction with living tissues. Some properties of sol–gel glasses (without Na), such as dissolution rate and bioactivity, have been compared with melt derived glasses [5,7,9,10]. Regarding this matter, one could wonder what would be the implication of Na addition in those sol–gel glasses? This is an open issue that is liable to investigation. In the case of materials containing crystalline phases to improve their mechanical properties, such as glass-ceramics, there are reasons to believe that the inclusion of Na_2O in their manufacturing process provides opportunities to enhance the mechanical strength, without losing biodegradability and their high bioactivity with the crystallization of certain sodium calcium silicate phases, as shown by Peitl et al. [22] already in 1997. Additionally, it would be very interesting to obtain glass-ceramic scaffolds suitable for tissue-engineering applications containing these highly bioactive phases by the sol–gel processing because this method has allowed the development of structures similar to that of trabecular bone (a spongy highly porous form of bone tissue) [3]. However, to the best of our knowledge, this has not been achieved yet.

Based on these observations, we began in 2007 a systematic study focusing on the synthesis of bioactive materials containing Na by different chemical methods. Preliminary results using a sol–gel route were presented in 2009 at the 15th International Sol–Gel Conference [23], where we discussed, among other things, about the synthesis and characterization of materials similar to the Bioglass® 45S5 and another biomaterial denominated Biosilicate®; a ~99.5% crystalline glass-ceramic of the $SiO_2–CaO–Na_2O–P_2O_5$ system that shows a similar chemical composition to Bioglass® 45S5 and also very high bioactivity [24–28]. Recently, we found only the work of Chen et al. [29] that also focuses on this same proposition. That work was accomplished in a period of time close to ours, in which the composition and the sol–gel route used were a little different from what we proposed. It is important to note that the objective of Chen et al. [29] was to obtain glass-ceramics, not both glasses and glass-ceramics. Thus, in order to explore this promising area of study, in this paper we focus on the synthesis and characterization of bioactive powders of the quaternary $SiO_2–CaO–Na_2O–P_2O_5$ system prepared by the sol–gel method showing similar composition to Bioglass® 45S5 and Biosilicate®, materials of this quaternary system that show the highest bioactivity indexes.

2. Materials and methods

2.1. Preparation of the gels

The preparation of the gels involved hydrolysis and polycondensation reactions of stoichiometric amounts of tetraethoxysilane (TEOS, $Si(OC_2H_5)_4$; Aldrich), triethylphosphate (TEP, $OP(OC_2H_5)_3$; Merck), and sodium ($NaNO_3$; Labsynth) and calcium ($Ca(NO_3)_2{\cdot}4H_2O$; Labsynth) nitrates, according to the established composition 49.15 mol% SiO_2:25.80 mol% CaO:23.33 mol% Na_2O:1.72 mol% P_2O_5 [22,30]. The hydrolysis of TEOS and TEP was catalyzed with a solution of 0.1 mol L^{-1} HNO_3 using the molar ratio $(HNO_3 + H_2O)/(TEOS + TEP) = 8$. Beginning with the hydrolysis of TEOS, the other reagents were sequentially added at 60-minute intervals, keeping the reaction mixture under constant stirring. Before reaching the gel point, the sols were poured into Teflon® tubes and stored for three days. In the end of this period, the gels were dried for seven days at 70 °C and two days at 130 °C. After completion of the drying step, the gels were manually crushed in an agate mortar, and powders with a particle size <150 μm were selected and characterized. All samples prepared with the use of TEP were identified as Bio1_TEP-Na. The same synthesis procedure was employed for the preparation of the gels involving the use of phosphoric acid (H_3PO_4; Qhemis). This set of samples was identified as Bio2_AFos-Na.

2.2. Conversion of the gels into ceramic powders

Just after milling, dried gels with particle size smaller than 150 μm were selected and individual portions containing approximately 20 g were placed in ZAS crucibles (ceramic material based on zirconia, alumina and silica) for heat treatment. The materials were heat-treated in an electric furnace at high temperatures under oxidizing atmosphere (air). The heating programs were determined using the analytical results of previous differential scanning calorimetry (DSC) and thermogravimetry (TG) analyses of the starting gels. The established thermal treatment programs consisted of heating with a 5 °C min^{-1} rate, followed by an isothermal heat treatment at temperature selected according to the data contained in Table 1. The cooling process of the samples in the electric furnace was natural.

After completion of the heat treatment program, the resulting powders were manually disaggregated in an agate mortar. Powders with particle sizes between 25 and 75 μm were selected and submitted to a series of analytical techniques proper for each specific material. Fig. 1 shows a flowchart that outlines the procedures established for particulate gel preparation, which were later characterized and submitted to different thermal treatments to obtain the ceramic powders.

Table 1
Heat treatment program for converting the Bio1_TEP-Na gels into ceramic materials.

*Sample	Final treatment temperature (°C)	Duration (min)
Bio1(1)_TEP-Na	700	180
Bio1(2)_TEP-Na	800	180
Bio1(3)_TEP-Na	900	180
Bio1(4)_TEP-Na	1000	180

*Samples derived from the Bio2_AFos-Na gels underwent the same heat treatments.

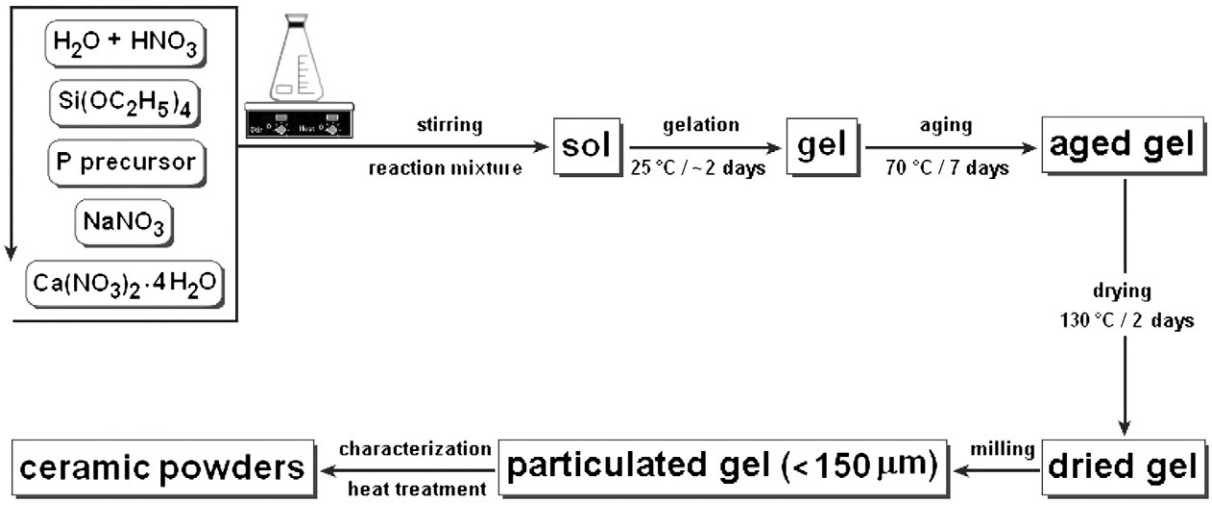

Fig. 1. Flowchart summary of the steps used to generate the particulate gels and their subsequent conversion into ceramic materials.

2.3. In vitro bioactivity tests

To evaluate the bioactivity of the synthesized materials, *in vitro* tests were performed according to the method described by Kokubo et al. [31]. The solution used to conduct this study, known as SBF (simulated body fluid), is acellular, protein-free and has a pH of 7.40. Table 2 shows the composition of this solution compared to human blood plasma [31]. It is important to mention that this solution is often used in the *in vitro* evaluation of the formation of a HA layer on the surface of materials designed for implants, according to ISO 23317, approved in June 2007 by the International Organization for Standardization [32].

2.3.1. Sample preparation

To test the *in vitro* bioactivity, the previously characterized powders with particle sizes between 25 and 75 μm were reformed as pellets 10 mm in diameter and 2.3 mm in height. This forming process consisted of two steps. First, the powders were uniaxially pressed without the addition of any agglutinant with 65 MPa for 6 min. The second stage was performed in an isostatic press at 170 MPa for 3 min. Soon after formation, each pellet was fixed along its circumference by a nylon string to allow for pellet suspension in the SBF solution during the test. The samples were cleaned for 15 s by ultrasound in acetone and, after drying, were soaked in polyethylene terephthalate bottles (PET) containing the SBF solution.

The volume of SBF used in bioactivity tests is related to the surface area of the sample. According to the procedures described by Kokubo et al. [31] for a dense material, the appropriate volume of solution should obey the following relationship:

$$V_s = S_a / 10 \quad (1)$$

where V_s represents the volume of SBF (mL) and S_a represents the total geometric area of the sample (mm^2). For porous materials, like the pressed powder pellets obtained in this study, those authors suggest the use of a volume higher than that calculated by the Eq. (1). Thus, in this work we used the following procedure: sample mass (m) divided by the volume of SBF (V_s) is equal to 0.01 g mL^{-1} because m was the same in all pellets.

During the tests, the samples were in contact with the SBF solution for periods of 3, 48, and 144 h, and the system temperature was maintained at 37 °C. After the test time required for each sample, they were removed from their bottles and immersed in acetone for 10 s to remove the SBF and stop surface reactions. After drying, both sample surfaces were analyzed to check for the formation of a superficial HA layer.

2.3.2. Evaluation of sample solubility in SBF

To evaluate the solubility of the samples in SBF solution during the bioactivity tests, the ionic concentrations of the species H^+, Ca^{2+} and $P—PO_4^{3-}$ were analyzed for each testing time. This evaluation was accomplished three times on average for each test time. Thus, it was possible to delineate the behavior of the *in vitro* bioactivity of the samples. Measurements of H^+ and Ca^{2+} species were performed employing the ion-selective electrode technique, using an electrolyte analyzer system Roche, model cobas b121. Ultraviolet and visible spectrophotometry (UV–Vis) were used for measurements of the species $P—PO_4^{3-}$, since the inorganic phosphate ions in solution react with certain compounds forming a blue chromophore, whose color intensity is proportional to its concentration in the medium [33,34]. A clinical analyzer system Siemens ADVIA® 1800 was employed to perform these measurements.

2.4. Instrumental analysis procedures

2.4.1. Differential scanning calorimetry and thermogravimetry (DSC/TG)

DSC and TG analyses were performed on a Netzsch STA 449C instrument under oxidizing atmosphere (synthetic air) with gas flow of 50 mL min^{-1}. Typical analysis involved samples of ~30 mg of the gel particles and a heating program with a rate of 5 °C min^{-1} from room temperature to 1000 °C to determine the initial heat treatment temperature and the onset of forming of the crystalline phases in the material.

2.4.2. X-ray diffraction (XRD)

The characterization of the crystalline phases resulting from the heat treatments of the gels was performed by XRD. We used a Siemens model D5000 diffractometer operating with CuKα radiation (λ = 0.15418 nm) and a filter system with a curved graphite secondary monochromator.

Table 2
Ionic concentration of human blood plasma and SBF solution proposed for the evaluation of *in vitro* bioactivity [31].

Simulated body fluid	Ionic concentration (mmol L^{-1})							
(SBF) ISO 23317	Na^+	K^+	Mg^{2+}	Ca^{2+}	Cl^-	HCO_3^-	HPO_4^{2-}	SO_4^{2-}
Human blood plasma	142.0	5.0	1.5	2.5	103.0	27.0	1.0	0.5
*SBF	142.0	5.0	1.5	2.5	147.8	4.2	1.0	0.5

*Buffer: tris(hydroxymethyl)aminomethane (TRIS).

The diffraction patterns were obtained in the 2θ range from 10° to 70°, in continuous mode at 2° min^{-1}.

2.4.3. Fourier transform infrared spectroscopy (FTIR)

The monitoring of pellet surface modifications after *in vitro* bioactivity tests was performed by FTIR using a spectrometer Perkin Elmer Spectrum GX model operating in reflectance mode with a 4 cm^{-1} resolution in the 4000–400 cm^{-1} region.

2.4.4. Scanning electron microscopy and microanalysis (SEM/EDS)

Morphological characterization of the pellets regarding the surface modifications that occurred during the *in vitro* bioactivity tests was performed by SEM. A set of samples was selected and analyzed before and after soaking in SBF solution at different testing times. The samples were coated with a thin evaporated gold layer, that makes the surface electro-conductive, and then analyzed under a Phillips FEG X-L30 microscope coupled to an energy dispersive X-ray spectroscopic analysis system (EDS), which aided the surface characterization through qualitative chemical analysis.

3. Results and discussion

3.1. Synthesis and characterization of the Bio1_TEP-Na and Bio2_AFos-Na samples

The gels of the SiO_2–CaO–Na_2O–P_2O_5 system synthesized using TEP and phosphoric acid revealed a gelation time of approximately 53 and 46 h, respectively. The time of gelation was considered as the time required for the reaction mixture to become relatively rigid and cease flowing. All gels obtained were transparent, colorless and optically homogeneous, as shown in Fig. 2.

Simultaneous DSC and TG analyses were performed with a fraction of the Bio1_TEP-Na gel particles to determine the best heat treatment programs. The results from these tests are shown in Fig. 3. The gels experienced three distinct mass loss steps and became virtually stable at approximately 600 °C. The first mass loss stage happened at ~120 °C, and is associated with the endothermic process of desorption of physically adsorbed water and alcohol [5,12,13]. The second happened at ~243 °C, and it is related to the volatilization of water by an exothermic chemical desorption process [13]. The third mass loss stage, which happened between 415 and 580 °C, was more pronounced. This stage is attributed to the evolution of the resulting sub-products from incomplete condensation of the precursors, and, mostly, the elimination of the nitrate ions, originated from $NaNO_3$ and $Ca(NO_3)_2{\cdot}4H_2O$ used in the gel preparation [5,12,13]. Another relevant observation was the exothermic final process, located near 803 °C, which is associated with the onset of crystallization.

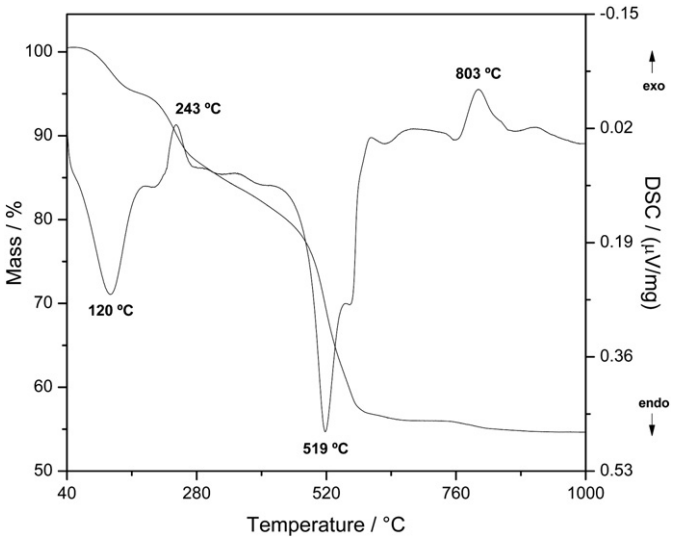

Fig. 3. DSC and TG curves of the Bio1_TEP-Na gel.

Based on the DSC and TG analyses, the initial heat treatment temperature was set to 700 °C and maintained for 3 h because in this temperature stability of the materials is already observed. Therefore, that condition should be sufficient for complete elimination of the nitrate ions, the last and most critical mass loss stage, in which maximum mass flow occurred from the solid to the vapor phase at 519 °C. Furthermore, that condition is suitable for generation of glassy materials, since crystallization is only observed in a non-isothermal DSC run at ~780 °C. However, after this relatively long heat-treatment at 700 °C all resulting materials were crystalline. Thus, other heat treatments were performed to monitor the sequence of phase formation with increasing temperature, such as those shown in Figs. 4 and 5. Heat treatments above 1000 °C were not performed since these materials melted at ~1069 °C (DSC curves not shown).

According to the X-ray diffractograms shown in Figs. 4 and 5, all sample sets exhibited the formation of the sodium calcium silicates $Na_2Ca_2Si_3O_9$ and $Na_2Ca_3Si_6O_{16}$ [35,36]. Probably, the phosphorus ions remained in solid solution in these crystal phases or in some minor fraction of a residual glass, since no other phase was evidenced containing this element. With increasing heat treatment temperature, the crystal phase $Na_2Ca_3Si_6O_{16}$ favored developed as shown by the intensity of their XRD peaks. On the other hand, the development of

Fig. 2. Illustration of Bio1_TEP-Na and Bio2_AFos-Na gels synthesized with the use of TEP and phosphoric acid as precursors of the P_2O_5 oxide, respectively.

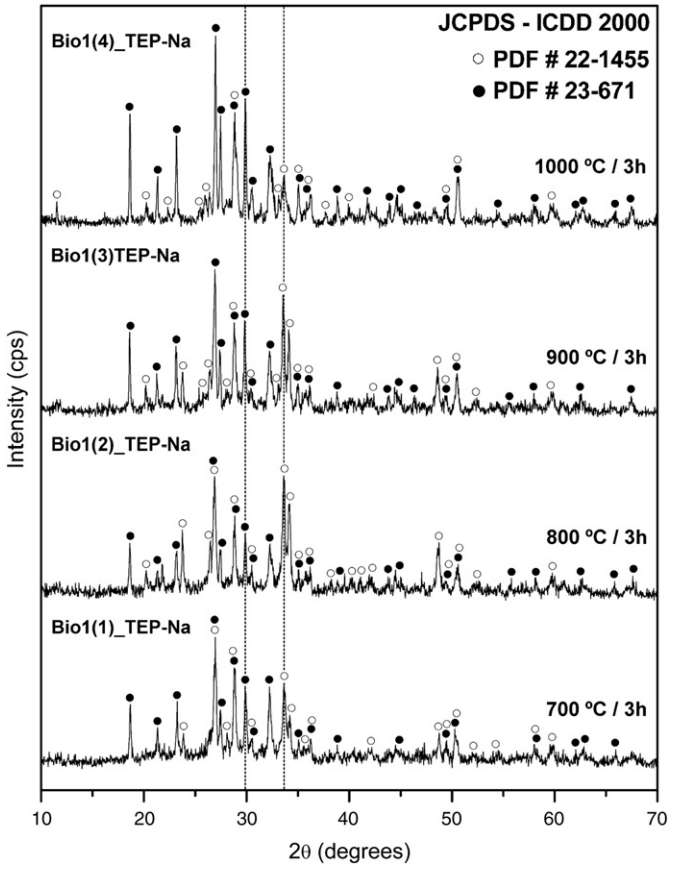

Fig. 4. XRD patterns of samples derived from Bio1_TEP-Na gel: ○ = $Na_2Ca_2Si_3O_9$; ● = $Na_2Ca_3Si_6O_{16}$.

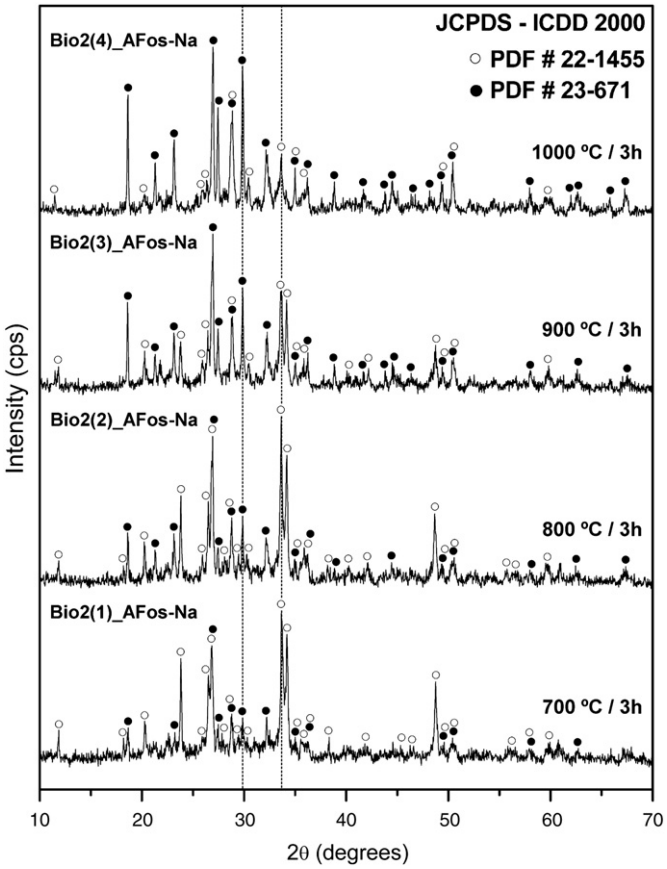

Fig. 5. XRD patterns of samples derived from Bio2_AFos-Na gel: ○ = $Na_2Ca_2Si_3O_9$; ● = $Na_2Ca_3Si_6O_{16}$.

the phase $Na_2Ca_2Si_3O_9$ was only detected for the temperatures of 700 and 800 °C. Above these temperatures the peaks of that phase considerably reduced. These tendencies can be better observed in the graphs in Fig. 6, in which the mineralization behavior of the Bio1_TEP-Na and Bio2_AFos-Na gels is qualitatively demonstrated. It is important to clarify that the graphs shown in Fig. 6 were constructed by monitoring an intense peak of each crystalline phase identified in X-ray diffractograms shown in Figs. 4 and 5 (these peaks were highlighted). Since the intensities of these peaks are directly related to the mass fraction of the existing phases, it was possible to monitor the increasing or decreasing tendencies of these phases as a function of the heat treatment temperature.

Comparing the graphs of the Bio1_TEP-Na and Bio2_AFos-Na sample sets in Fig. 6, we observe similar mineralization sequences for both sets with increasing heat treatment temperature. However, an interesting feature of the samples derived from the Bio2_AFos-Na gel, which, differently for the samples derived from the Bio1_TEP-Na gel, as result of the heat treatment performed at 700 °C, exhibited preferential formation of the highly bioactive crystal phase $Na_2Ca_2Si_3O_9$.

3.2. In vitro bioactivity tests

The morphologies of the samples originating from the gels Bio1_TEP-Na and Bio2_AFos-Na, and their respective qualitative chemical analysis, before and after exposure to SBF solution at different testing times, are shown in Figs. 7 and 8. Significant superficial changes in relation to the morphology and chemical composition of the samples could only be observed from the tests of 48 h. The samples submitted to these test conditions exhibited the typical morphology of HA in an advanced state [11,12,31], but still with spaced granules that do not cover all the sample surfaces. This fact was more pronounced in the samples subjected to heat treatment at 1000 °C as shown in Figs. 7 (items b and c) and 8, respectively. Fig. 7 (item d) shows the morphology of a sample exposed to SBF for 144 h. From this example it is possible to observe that the formed HA layer is more homogeneous and exhibits larger granules than the ones formed in the samples of 48 h of testing. According to this morphology, the formation of HA was already well established and grew with increased test time.

The development of the formed HA layer on the surface of these materials can also be followed in the EDS spectra. As observed in the spectra of Bio1(3)_TEP-Na and Bio2(3)_AFos-Na, shown in Fig. 7, a large compositional change occurred on their surfaces after 48 h of testing. Even with increasing migration of Ca and P to the surface of these samples, the presence of Si is still very evident, which can be explained by the low density of the formed HA layer, allowing, thus, the detection of the existing Si on the surface immediately below this layer. This is clear for the Bio2(4)_AFos-Na sample, shown in Fig. 8, where it was possible to analyze an area that had not been fully covered by HA. For the samples with 144 h of testing, it was not possible to observe the presence of Si, while the presence of Ca and P became almost exclusive. Thus, it is reasonable to conclude that for 144 h of testing all the samples were completely covered by a HA layer.

The FTIR spectra of all samples, before and after exposure to SBF solution for 3, 48 and 144 h, are shown in Fig. 9. Before these tests, all samples exhibited a spectrum characterized by the presence of bands in the region between 1180 and 940 cm^{-1}, associated with the vibrational mode of the νSi—O bonds. Bands related to the vibrational mode of the δSi—O—Si bonds were identified near 643, 555 and 485 cm^{-1} (the band at 485 cm^{-1} being more intense). It is important to note that in the spectrum of the samples Bio2(1)_AFos-Na and Bio2(2)_AFos-Na, the band located at 555 cm^{-1} was much more intense.

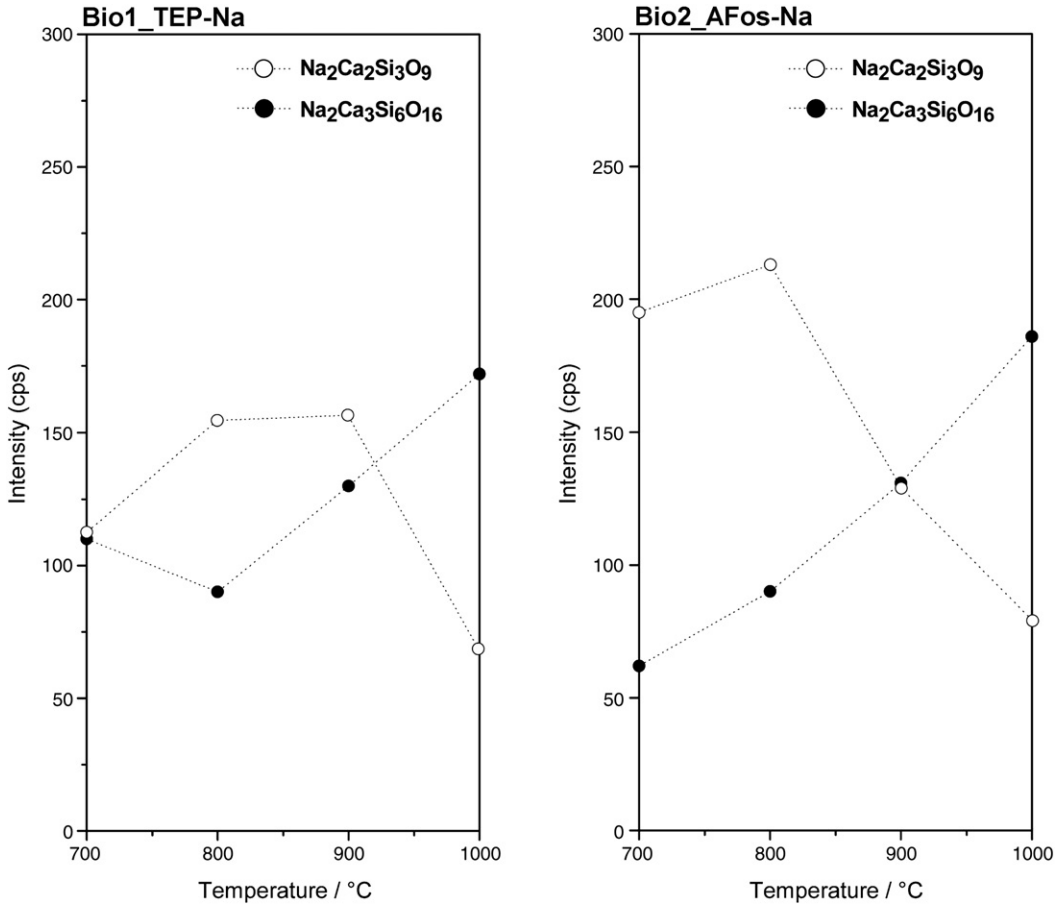

Fig. 6. Mineralization of the Bio1_TEP-Na and Bio2_AFos-Na gels as a function of heat treatment temperature.

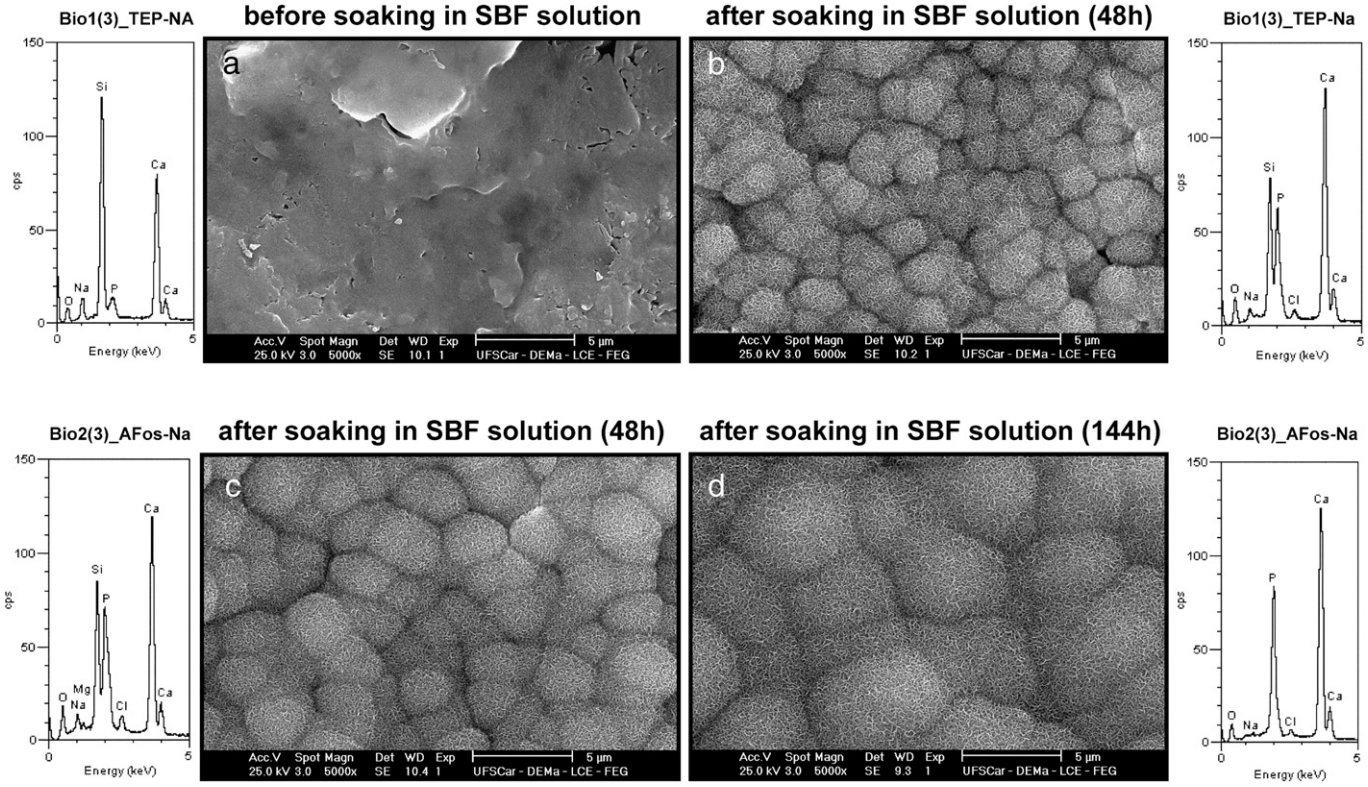

Fig. 7. SEM micrographs and EDS spectra of Bio1(3)_TEP-Na and Bio2(3)_AFos-Na sample surfaces: (a) before the test; (b) and (c) after 48 h; (d) after 144 h.

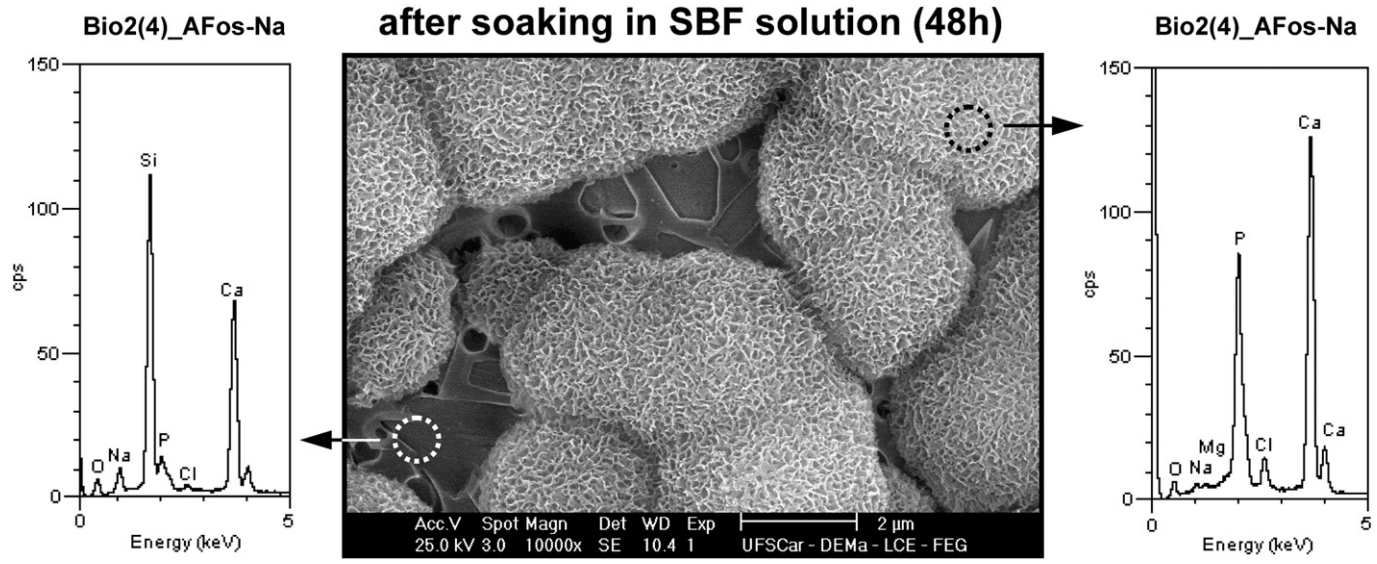

Fig. 8. SEM micrographs and EDS spectra of the Bio2(4)_AFos-Na sample surface after 48 h of testing.

The configuration of these spectra is characteristic of the crystal phase $Na_2Ca_2Si_3O_9$ [24,30], which is consistent with the X-ray diffractograms demonstrated in Fig. 5, which show the preferential formation of this phase at 700 and 800 °C, respectively.

According to the FTIR spectra of the samples exposed to SBF solution, it is possible to note that, after 3 h of testing, a significant change occurred only on the surface of samples Bio2(1)_AFos-Na and Bio2(2)_AFos-Na, being characterized by the deformation of the bands related to Si—O and

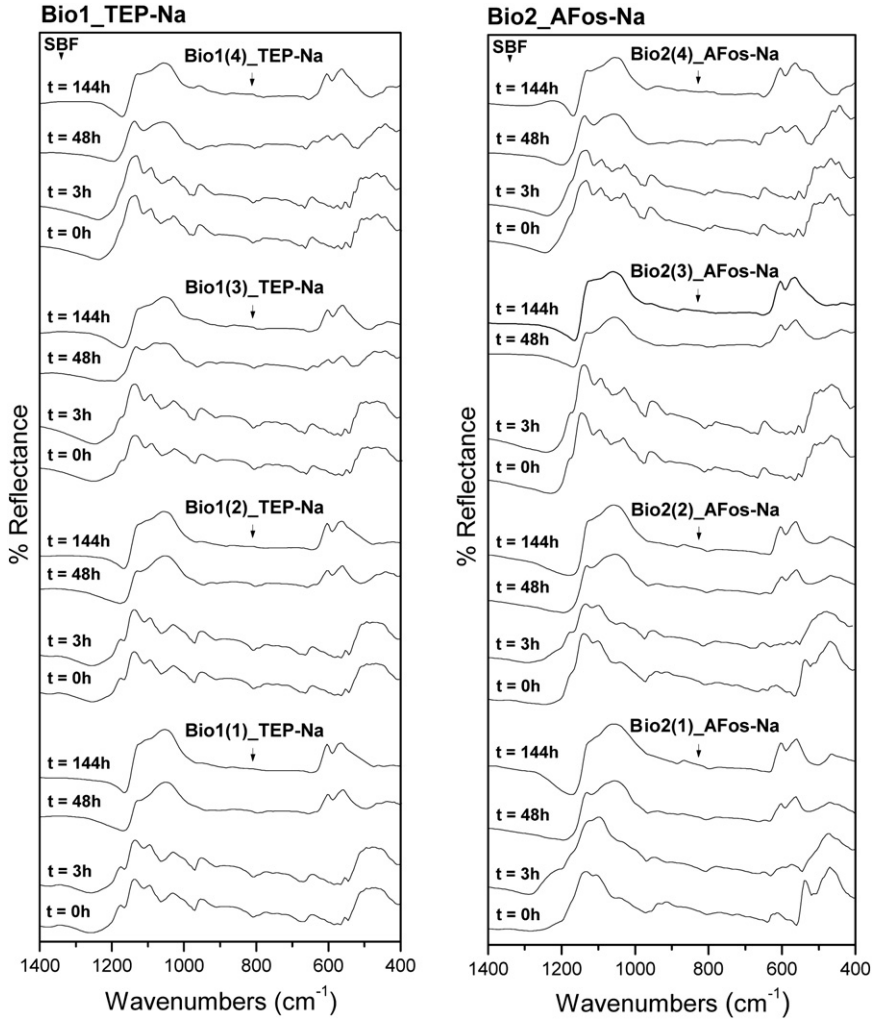

Fig. 9. FTIR spectra of all sample surfaces before and after soaking in SBF solution at different testing times.

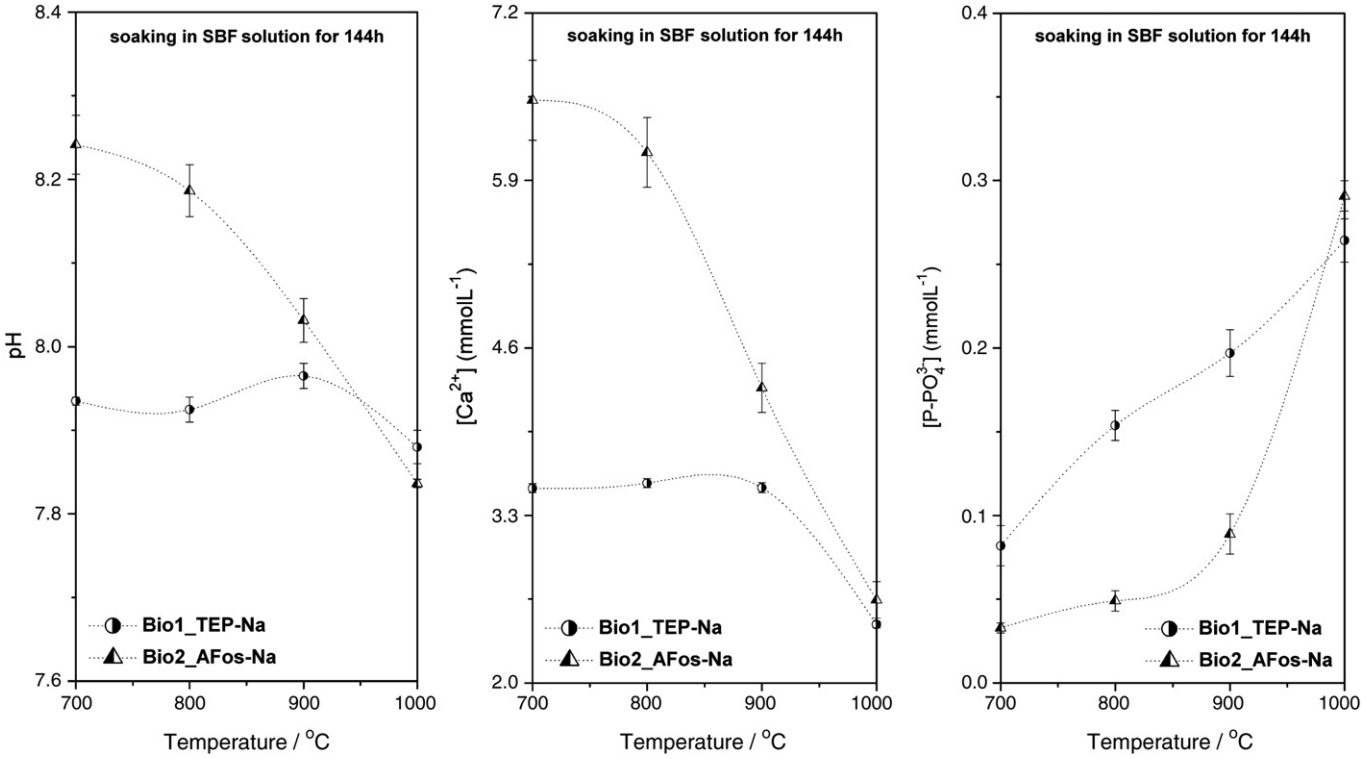

Fig. 10. Variation in pH and calcium and phosphorus concentrations after 144 h exposure of the samples to SBF solution.

Si—O—Si located at approximately 1060 and 550 cm^{-1}, respectively. These changes in the spectra can be attributed to the stages 1 and 2 of the proposed mechanism for bioactivity, in which culminates the formation of a silica-rich layer on the sample surfaces [2,3,9,24,30]. These initial modifications verified on these sample surfaces certainly occurred for all the others, however, for longer times than 3 h. This result by itself already indicates that the phase $Na_2Ca_3Si_6O_{16}$ is more stable, since it is present in these other samples in more significant amounts than in the samples Bio2(1)_AFos-Na and Bio2(2)_AFos-Na. From the testing of 48 h, all the obtained spectra were analog to the synthetic HA spectrum, exhibiting, as a function of the time of testing, only changes referring to the intensity of the typical HA bands, located near 1130, 1055, 605 and 565 cm^{-1} [5,11,12,24,30]. The observed increase of the intensity of these bands is associated to the higher density of the formed HA layer on the sample surfaces. This fact could be also monitored in the SEM micrographs and EDS spectra as shown in Figs. 7 and 8.

3.2.1. Evaluation of sample solubility in SBF

The variations of pH and calcium and phosphorus concentrations after 144 h of exposure of all samples to SBF solution are compared as a function of treatment temperature in Fig. 10. In general, all the obtained materials exhibited a higher stability in SBF solution with the increase of the heat treatment temperature. Since the reactivity of these materials is related to the crystalline phases present and their crystallized fractions (and also to a possible residual glassy fraction), it is possible to say that the phase $Na_2Ca_3Si_6O_{16}$ confers greater stability to these materials because its fraction present in the prepared samples at higher temperatures was superior than the $Na_2Ca_2Si_3O_9$ phase, which is recognized by its high bioactivity [22–30].

For the samples obtained at 1000 °C, which had preferential formation of $Na_2Ca_3Si_6O_{16}$, the variation of the concentration of the species Ca^{2+} and $P—PO_4^{3-}$ in the SBF solution was not very accentuated when compared to the other samples, being around 0.24 and 0.70 mmol L^{-1}, respectively. The pH of the solution followed the same tendency, since its variation is due to the ionic exchange between the species H^+ and Ca^{2+}. Due to the low solubility of these samples, there was no meaningful increase in the concentration of Ca^{2+} ions in the solution, then the pH has not changed much either. On the other hand, the samples obtained at 700, 800 and 900 °C revealed to be much more reactive, mainly those derived from the gel Bio2_AFos-Na. For these samples, the highest activity of the species H^+, Ca^{2+} and $P—PO_4^{3-}$ can be related to the presence of the crystal phase $Na_2Ca_2Si_3O_9$, that, in this case, exhibited X-ray peaks (Figs. 4 and 5) with similar intensities to the $Na_2Ca_3Si_6O_{16}$ phase. In the specific case of the Bio2(1)_AFos-Na and Bio2(2)_AFos-Na samples, in which the formation of the $Na_2Ca_2Si_3O_9$ phase occurred in a preferential manner, major changes in the concentration of the SBF solution occur, with the pH reaching values

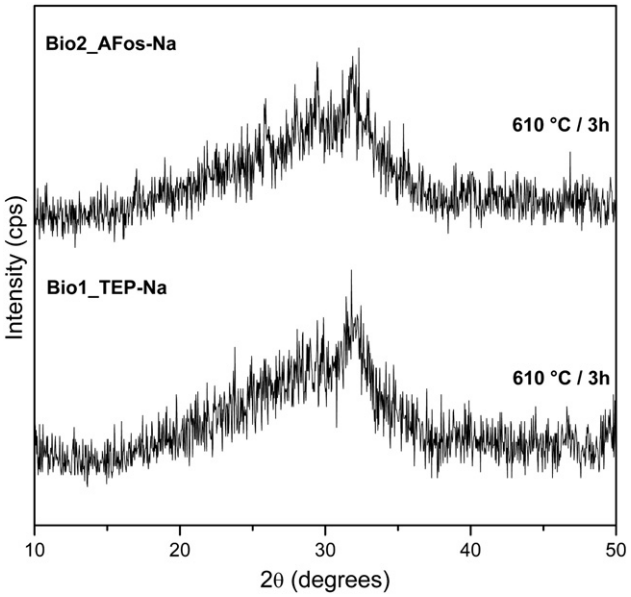

Fig. 11. XRD patterns of Bio1_TEP-Na and Bio2_AFos-Na samples derived from heat treatment at 610 °C.

around 8.2. The variation of Ca^{2+} ions was around 3.77 mmol L^{-1}, while the variation of the species P—PO_4^{3-}, which is related to its reduction in the solution due to the early formation of an amorphous calcium phosphate layer on the surface of materials and its subsequent evolution to HA [2,3,9,24,30], was around 0.96 mmol L^{-1}. This particular value corresponds to the almost total consumption of the species P—PO_4^{3-}, since the SBF solution used in the tests contained an initial concentration 1.0 mmol L^{-1} (see Table 2).

3.3. Final considerations

According to the results obtained with the conversion of the Bio1_TEP-Na and Bio2_AFos-Na gels into ceramic materials, it was clear that the choice of the first heat treatment for 3 h at 700 °C (based on the results of the analysis of DSC and TG — Fig. 3) was not appropriate to obtain glassy materials. Instead, an extensive temperature range and treatment times must be chosen for this purpose, since these materials are virtually stable from approximately 600 °C and the onset of crystallization was only evidenced at ~780 °C. Thus, in the present work a single heat treatment was performed at 610 °C for 3 h to evaluate the behavior of the Bio1_TEP-Na and Bio2_AFos-Na gel samples under this condition. Fig. 11 shows the X-ray diffractograms of the resulting materials.

The X-ray diffractograms of the samples treated at 610 °C exhibit predominantly amorphous character, but a beginning of crystallization can be detected. These results indicate the possibility of obtaining this important biomaterial in the glassy state, as well as the pursuit for the isolation of the crystal phase $Na_2Ca_2Si_3O_9$, which is known to be highly bioactive. Hence, the temperature and treatment time to which samples are to be submitted could be further explored. In the case of glassy materials, attention should be given to the removal of the nitrate ions (species that require higher temperature for elimination). The use of other CaO and Na_2O precursors containing counter ions of easy removal should also be considered. In order to obtain glass-ceramics containing only the crystal phase $Na_2Ca_2Si_3O_9$, as recently reported to Chen et al. [29], a small modification in the sol–gel route or/and composition proposed here will be necessary.

4. Conclusions

Crystalline bioactive powders of the SiO_2–CaO–Na_2O–P_2O_5 system were synthesized by the sol–gel method. The syntheses were performed using two different P_2O_5 precursors: triethylphosphate and phosphoric acid. The alternation of these precursors significantly affected the properties of the resulting materials, especially gel mineralization during thermal treatment, but all were proven to be bioactive, as demonstrated by the formation of a hydroxyapatite layer on their surfaces during *in vitro* tests. The samples prepared using phosphoric acid exhibited the best bioactivity. This was attributed to the preferential formation of crystalline sodium calcium silicate $Na_2Ca_2Si_3O_9$, especially in the samples submitted to the heat treatment at 700 and 800 °C, a fact not evidenced in the samples prepared using triethylphosphate.

So far it has not been possible to obtain fully glassy materials, however the precipitation of the highly bioactive crystal phase $Na_2Ca_2Si_3O_9$ (although not in isolated form) was a very significant result. With the sol–gel route established in this work we demonstrated the formation of this desirable phase in much milder laboratory conditions than the conventional glass-ceramic route involving melting/cooling and subsequent crystallization.

Acknowledgments

We thank the Brazilian funding agencies Coordenação de Aperfeiçoamento de Pessoal de Nível Superior (CAPES) for the *MSc* scholarship to Renato L. Siqueira, and Conselho Nacional de Desenvolvimento Científico e Tecnológico (CNPq) and Fundação de Amparo à Pesquisa do Estado de São Paulo (FAPESP) grant number #2007/08179-9 for financial support of this research project. We also thank Vitrovita (Glass-Ceramic Innovation Institute, São Carlos — SP, Brazil) for the use of their equipment.

References

[1] L.L. Hench, J. Mater. Sci. Mater. Med. 17 (2006) 967–978.
[2] L.L. Hench, J. Am. Ceram. Soc. 81 (1998) 1705–1728.
[3] J.R. Jones, E. Gentleman, J. Polak, Elements 3 (2007) 393–399.
[4] L.L. Hench, J. Eur. Ceram. Soc. 29 (2009) 1257–1265.
[5] R. Li, Sol–gel processing of bioactive glass powders, Dissertation (Doctor of Philosophy), University of Florida, 1991.
[6] S. Sakka, Handbook of Sol–gel Science and Technology: Processing, Characterization and Applications, Vol. 1 (Sol–gel Processing), Kluwer Academic Publishers, New York, 2005.
[7] P. Sepulveda, J.R. Jones, L.L. Hench, J. Biomed. Mater. Res. 58 (2001) 734–740.
[8] R. Li, A.E. Clark, L.L. Hench, Alkali-free bioactive sol–gel compositions, Patent International Publication Number WO1991/017965, 1991.
[9] D. Arcos, D.C. Greenspan, M. Vallet-Regí, J. Biomed. Mater. Res. 65 (2003) 344–351.
[10] P. Sepulveda, J.R. Jones, L.L. Hench, J. Biomed. Mater. Res. 61 (2002) 301–311.
[11] M. Vallet-Regí, V.R. Rangel, A.J. Salinas, Eur. J. Inorg. Chem. 2003 (2003) 1029–1042.
[12] I. Izquierdo-Barba, A.J. Salinas, M. Vallet-Regí, J. Biomed. Mater. Res. 47 (1999) 243–250.
[13] A. Oki, B. Parveen, S. Hossain, S. Adeniji, H. Donahue, J. Biomed. Mater. Res. 69 (2003) 216–221.
[14] A. Balamurugan, G. Balossier, S. Kannan, J. Michel, A.H.S. Rebelo, J.M.F. Ferreira, Acta Biomater. 3 (2007) 255–262.
[15] A. Balamurugan, G. Balossier, J. Michel, S. Kannan, H. Benhayoune, A.H.S. Rebelo, J.M.F. Ferreira, J. Biomed. Mater. Res. 83 (2007) 546–553.
[16] A. Saboori, M. Rabiee, F. Moztarzadeh, M. Sheikhi, M. Tahriri, M. Karimi, Mater. Sci. Eng. C 29 (2009) 335–340.
[17] A. Balamurugan, G. Balossier, D. Laurent-Maquin, S. Pina, A.H.S. Rebelo, J. Faure, J.M.F. Ferreira, Dent. Mater. 24 (2008) 1343–1351.
[18] J. Lao, E. Jallot, J.-M. Nedelec, Chem. Mater. 20 (2008) 4969–4973.
[19] W.S. Roberto, M.M. Pereira, T.P.R. Campos, Mater. Res. 6 (2003) 123–127.
[20] M. Łączka, K. Cholewa-Kowalska, A. Łączka-Osyczka, M. Tworzydlo, B. Turyna, J. Biomed. Mater. Res. 52 (2000) 601–612.
[21] D. Carta, D.M. Pickup, J.C. Knowles, M.E. Smithc, R.J. Newporta, J. Mater. Chem. 15 (2005) 2134–2140.
[22] O. Peitl, E.D. Zanotto, La Torre, G. P., L.L. Hench, Bioactive ceramics and method of preparing bioactive ceramics, International Publication Number WO/1997/041079, 1997.
[23] R.L. Siqueira, O. Peitl, E.D. Zanotto, 15th International Sol–Gel Conference, Porto de Galinhas, Brazil, 2009, 2009, p. 301.
[24] J. Moura, L.N. Teixeira, C. Ravagnani, O. Peitl, E.D. Zanotto, M.M. Beloti, H. Panzeri, A.L. Rosa, P.T. Oliveira, J. Biomed. Mater. Res. 82 (2007) 545–557.
[25] R.N. Granito, D.A. Ribeiro, A.C.M. Renno, C. Ravagnani, P.S. Bossini, O. Peitl, E.D. Zanotto, N.A. Parizotto, J. Oishi, J. Mater. Sci. Mater. Med. 20 (2009) 2521–2526.
[26] E.T. Massuda, L.L. Maldonado, J.T. Lima Júnior, O. Peitl, M.A. Hyppolito, J.A. Oliveira, Braz. J. Otorhinolaryngol. 75 (2009) 665–668.
[27] V.M. Roriz, A.L. Rosa, O. Peitl, E.D. Zanotto, H. Panzeri, P.T. Oliveira, Clin. Oral Implants Res. 21 (2010) 148–155.
[28] A.C.M. Renno, P.A. McDonnell, M.C. Crovace, E.D. Zanotto, L. Laakso, Photomed. Laser Surg. 28 (2010) 131–133.
[29] Q.-Z. Chen, Y. Li, L.-Y. Jin, J.M.W. Quinn, P.A. Komesaroff, Acta Biomater. 6 (2010) 4143–4153.
[30] O. Peitl, E.D. Zanotto, L.L. Hench, J. Non-Cryst. Solids 292 (2001) 115–1126.
[31] T. Kokubo, H. Takadama, Biomaterials 27 (2006) 2907–2915.
[32] ISO 23317, Implants for Surgery: *In Vitro* Evaluation for Apatite-forming Ability of Implant Materials, , 2007.
[33] C.H. Fiske, Y. Subbarow, J. Biol. Chem. 66 (1925) 375–400.
[34] G. Gomori, J. Lab. Clin. Med. 21 (1942) 955–960.
[35] Powder diffraction file, nº 22–1455 (JCPDS – ICDD 2000).
[36] Powder diffraction file, nº 23–671 (JCPDS – ICDD 2000).